VALIDATION OF THE DEVELOPED TRIAXIAL NONLINEAR MATERIAL MODEL FOR CONCRETE

Mirela Galić[1] – Pavao Marović[1*]

[1]Chair for Strength of Materials and Testing of Structures, Faculty of Civil Engineering, Architecture and Geodesy, University of Split, Matice hrvatske 15, HR-21000 Split, Croatia

ARTICLE INFO

***Article history*:**
Received: 9.3.2016.
Received in revised form: 2.5.2017.
Accepted: 8.5.2017.

Keywords:
Material model
Nonlinearity
Triaxial stress state
Concrete
Numerical analysis
Validation

Abstract:

This paper presents a validation of newly developed material model for concrete. The model is based on a combination of elasto-fracture-plastic formulation, considering all dominant influences in concrete: yielding in compression, fracture in tension, softening and hardening. The modified Mohr-Coulomb criterion for dominant compression stresses, the modified Rankine criterion for dominant tension stresses, exponential softening and the function for hardening are considered in this model. All constitutive equations are defined by elementary material parameters (Young's modulus of elasticity, Poisson's coefficient, maximal uniaxial tensile and compression stresses, the coefficient of tensile correction, maximal tensile and maximal compression strains). A multi-surface presentation of the model is implemented which permits the rapid convergence of the mathematical procedure. The model uses return-mapping algorithm for the integration of the constitutive equations with associated and non-associated flow rules. Considering triaxial stress state, the paper presents the structural validation of a developed numerical model, which is incorporated into computer programme PRECON3D, illustrated on four examples, both experimental and numerical, taken from the literature: (i) four point bending of normal-strength and high-strength reinforced concrete beams with four different constant-zone lengths and two different reinforcement ratios; (ii) three point bending of reinforced concrete beam; (iii) prestressed concrete beam; (iv) prestressed Π-beam.

1 Introduction

Some time ago, we developed a computer programme called PRECON3D [1] and [2], for a three-dimensional non-linear analysis of reinforced and prestressed concrete structures where the structures are discretized by three-dimensional finite elements with an embedded one-dimensional

* Corresponding author.
E-mail address: pavao.marovic@gradst.hr

element of reinforcement and prestressed tendons. Non-linear triaxial behaviour of concrete is involved in the material model, including all dominant influences in concrete (yielding in compression, fracture in tension, softening and hardening) [3]. The non-linear behaviour of reinforcement and prestressed tendons is described by the one-dimensional elasto-viscoplastic model. The perfect or full bond is assumed, but the bond-slip effect is not included. The tendon element geometry is described by the second order space function which is determined by its projections [4].
The reason for doing that were the following phenomena which have been noticed performing the analyses of prestressed concrete structures: non-linear and non-elastic behaviour, damage causing degradation of linear-elastic matrix constants, non-linear behaviour after peak stress, multiaxial and non-linear distribution of strain causing the development of cracks, hardening of non-cracked concrete between two cracks, interface of concrete and reinforcement bars, distinctly triaxial stresses around the anchors. Due to this highly complex behaviour, prestressed beams are exposed to various expensive experimental tests before being embedded in a structure. An appropriate numerical model for describing distinctly non-linear triaxial behaviour of concrete and an accurate description of geometry allow the analysis of these structures via numerical tests.
In the first part of the paper, the main constitutive equations of the fracture and plastic models, i.e. a non-linear triaxial behaviour of concrete [5] will be presented, which is involved in the material model, including all dominant influences in concrete (yielding in compression, fracture in tension, softening and hardening).
In the second part of the paper, a computer programme PRECON3D [1], which can be used very simple because the material model is defined by elementary material parameters (Young's modulus, Poisson's coefficient, maximal uniaxial tensile and compression stresses, coefficient of tensile correction, maximal tensile and maximal compression strains) will be presented through numerical testing of the prestressed concrete girders from the engineering practice.
Therefore, the paper presents the structural validation of developed numerical model, PRECON3D [1], on a few examples and the obtained results will be compared with the known numerical and experimental ones. Furthermore, from the performed numerical analyses, it will be concluded that the presented programme and numerical model can be effectively used in nonlinear analysis of reinforced and prestressed concrete structures.

2 Developed numerical model

Nonlinear behaviour of concrete is described by an elasto-plastic modified material model which is based on the Mohr-Coulomb law for dominant compression stresses and the Rankine law for dominant tensile stresses, [2] and [3]. A multi-surface presentation of the model (Fig. 1) is implemented in the model, enabling thus a rapid convergence of the mathematical procedure. The non-linear, triaxial behaviour of concrete is included in this model, with all dominant influences in concrete such as yielding in compression, cracking in tension, softening and hardening of concrete.

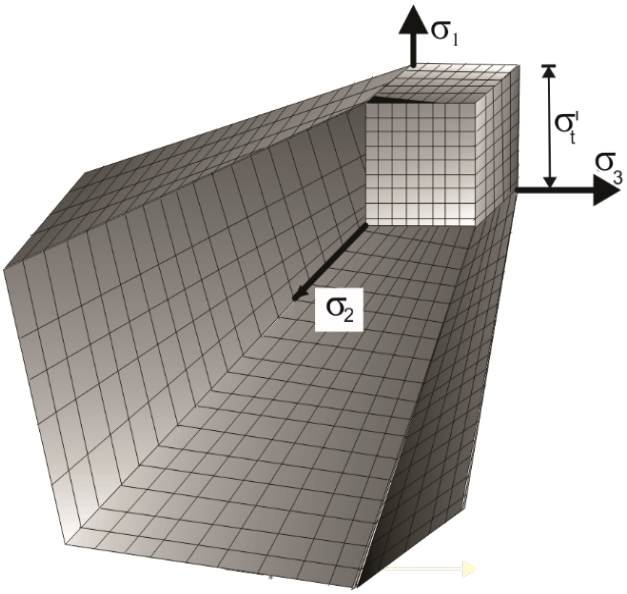

Figure 1. Multi-surface presentation of material model for concrete.

For the description of all of these parameters, it is necessary to define: (a) a fracture model for concrete with the tensile softening of cracked concrete and stress-strain relation of cracked concrete; (b) a plasticity model for concrete with softening and hardening with respect to the total plastic strain.

2.1 Fracture model for concrete

Previous research papers have shown that one of the most reliable material laws for describing the behaviour of concrete under dominant tensile stresses is the Rankine material law. This law has been chosen for the application given that it has a simple mathematical interpretation and its predictions have proven to agree well with experimental results.

According to the Rankine material law, concrete softens in tension when at least one principal tensile stress reaches the tensile strength of concrete. In the domains where the compressive stress (σ_c) appears, the experiments have determined that the tensile strength depends also on the magnitude of those compressive stresses [6]. Consequently, it is necessary to reduce the tensile strength which depends on the number of compressive stresses in the considered domain. In Fig. 2, σ^{red} is the reduced tensile strength, σ_i (i = 1, 2, 3) are the principal tensile stresses in the considered directions, and σ'_c is the compressive strength of concrete. After the appearance of the first crack, it is assumed that its direction will stay fixed for the following load increments and that the following cracks will appear perpendicularly to the first one.

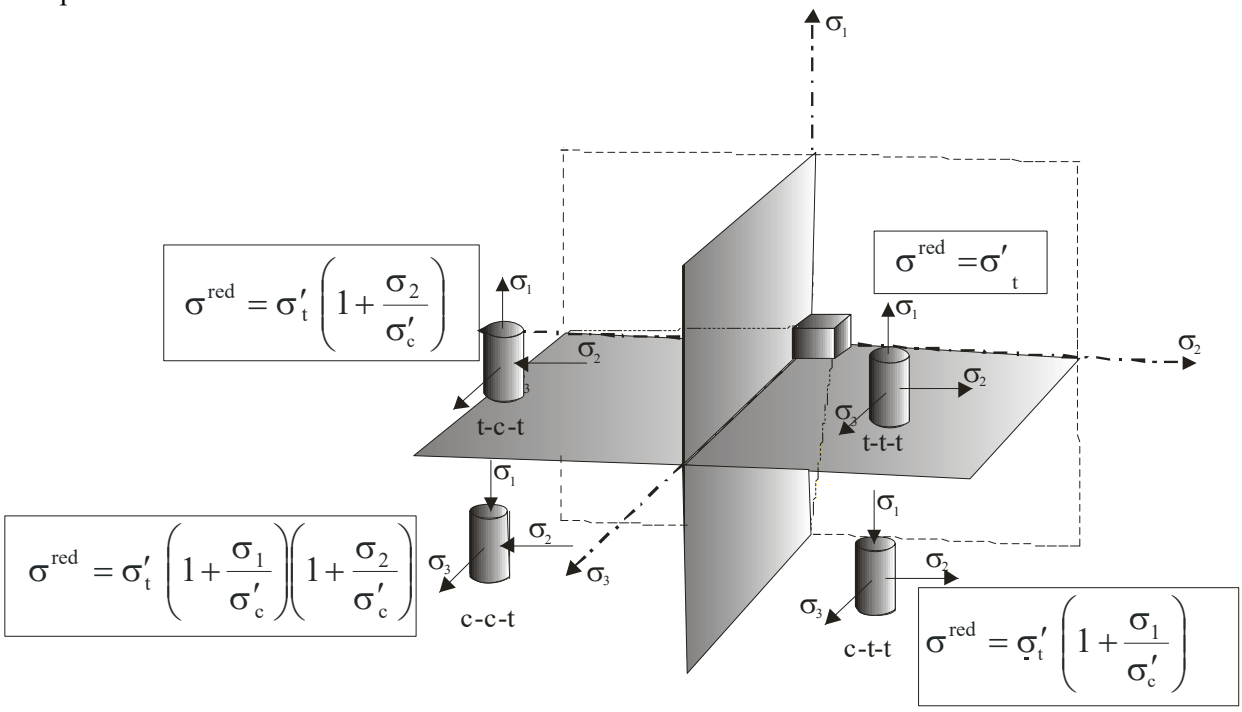

Figure 2. Final reduction of normal stresses and plane of cracking in all combinations for compressive and tensile behaviour in eight octahedral (tension-tension-tension (t-t-t), t-t-c, t-c-t, t-c-c, c-t-t-, c-t-t, c-c-t, and compression-compression-compression (c-c-c)).

In the considered model, the tensile softening is simulated by the linear decrease of tensile stresses perpendicular onto crack plane as shown in Fig. 3 with the variations of modulus of elasticity during the loading (Fig. 3(a)) and unloading (Fig. 3(b)) paths of cracked concrete.

The value of parameter ω is taken to be 0.5 according to [7].

The applied model assumes that the loading, unloading and reloading paths of cracked concrete follow the linear constitutive law with a fictitious modulus of elasticity defined by:

$$E_i^* = \alpha \sigma_t' \frac{1 - \frac{\varepsilon_i}{\varepsilon_{t\max}}}{\varepsilon_i} \qquad (1)$$

where α and ε_{tmax} are parameters defining tensile softening and ε_i is the maximal tensile strain in the observed Gaussian point, which is remembered for any integration point and any crack direction. As the material behaviour changes in correlation with the parameter α, the changes are relatively small, and it is recommended to use α = 0.6 according to [8]. The

parameter α can be considered as an artificial material characteristic as:

$$\alpha = \frac{G_f}{l_c \, \sigma_t^i} \tag{2}$$

taking into account fracture energy, G_f, characteristic length of the sampling point, l_c, and the uniaxial tensile strength of concrete, σ_t'.

Three significant moments are monitored: (i) the appearance of the first crack that reduces the appropriate coefficients of the material constant matrix; (ii) the appearance of the second crack at the same integration point (perpendicularly to the first crack), which again reduces the appropriate coefficients; (iii) the appearance of the third crack at the same integration point perpendicularly to the first two cracks.

In modelling the stress-strain relation of cracked concrete, it is assumed that the concrete changes from isotropic to orthotropic material with its axis oriented toward the maximal tensile stress (Fig. 4).

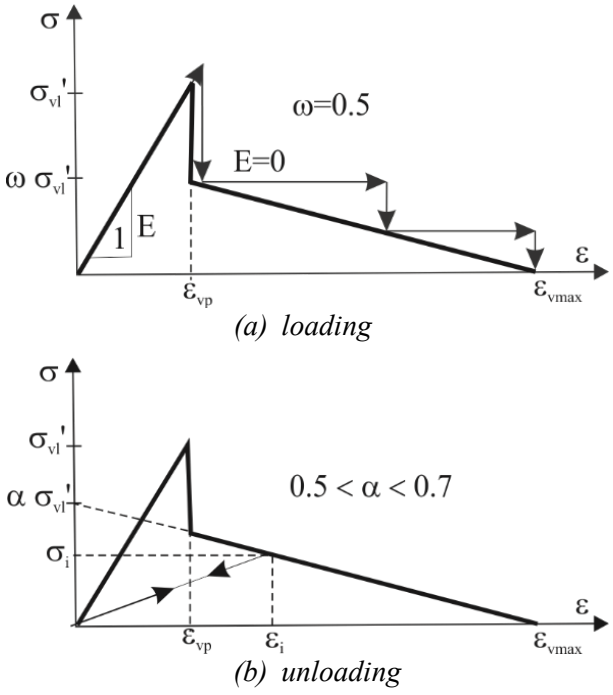

Figure 3. Tensile stiffening model for cracked concrete: (a) loading; (b) unloading.

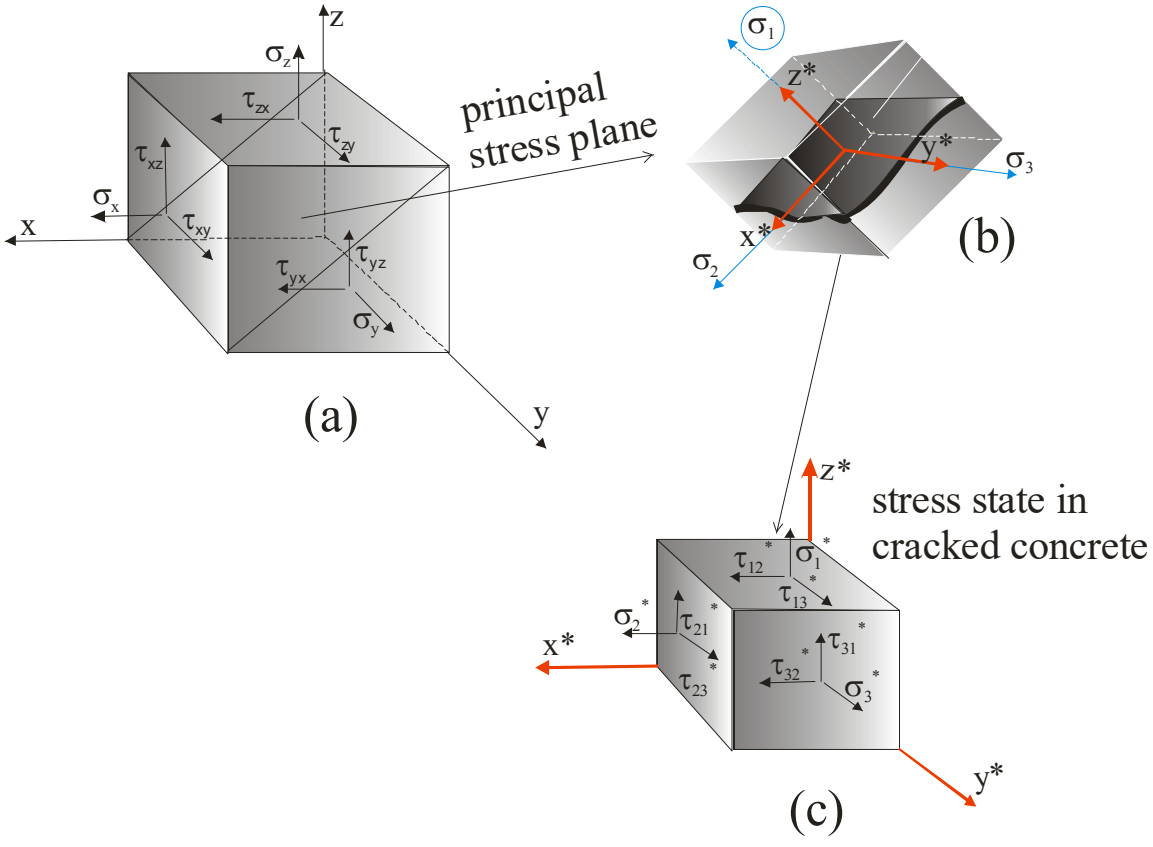

Figure 4. Stress states: (a) initial stresses in the Cartesian coordinate system; (b) principal stresses; (c) stresses in the cracked concrete defined in a local coordinate system x-y*-z*.*

It is also assumed that a crack is formed in the plane perpendicular to principal tensile stresses which are assumed to be greater than the tensile strength or the reduced tensile strength of concrete, depending on the domain where the stresses have been calculated. In such a coordinate system, a constitutive stress-strain increment relation is considered and afterwards transferred into a global coordinate system. The stress state defined in the global coordinate system *x-y-z* is mapped onto the plane of the crack. In this plane a new coordinate system *x*-y*-z** is formed in which the constitutive law of the stress-strain relation is established. It can be noticed that this local coordinate system coincides with the coordinate system of the principal stresses at the moment of the formation of the first crack (Fig. 4).

The matrix **D*** is the material matrix of the cracked concrete which, in the case of the appearance of one crack (e.g. in the direction 1), is defined as:

$$\mathbf{D}^{*}=\begin{vmatrix} \frac{E_1^{*}(1-\nu)}{(1+\nu)(1-2\nu)} & 0 & 0 & 0 & 0 & 0 \\ 0 & \frac{E(1-\nu)}{(1+\nu)(1-2\nu)} & \frac{E\,\nu}{(1+\nu)(1-2\nu)} & 0 & 0 & 0 \\ 0 & \frac{E\,\nu}{(1+\nu)(1-2\nu)} & \frac{E\,(1-\nu)}{(1+\nu)(1-2\nu)} & 0 & 0 & 0 \\ 0 & 0 & 0 & G_{12}^{*} & 0 & 0 \\ 0 & 0 & 0 & 0 & G_{23}^{*} & 0 \\ 0 & 0 & 0 & 0 & 0 & G_{31}^{*} \end{vmatrix} \tag{3}$$

whereas in the case of the appearance of two cracks (e.g. in the directions 1 and 2), it is defined as:

$$\mathbf{D}^{**}=\begin{vmatrix} \frac{E_1^{*}(1-\nu)}{(1+\nu)(1-2\nu)} & 0 & 0 & 0 & 0 & 0 \\ 0 & \frac{E_2^{*}(1-\nu)}{(1+\nu)(1-2\nu)} & 0 & 0 & 0 & 0 \\ 0 & 0 & \frac{E\,(1-\nu)}{(1+\nu)(1-2\nu)} & 0 & 0 & 0 \\ 0 & 0 & 0 & G_{12}^{*} & 0 & 0 \\ 0 & 0 & 0 & 0 & G_{23}^{*} & 0 \\ 0 & 0 & 0 & 0 & 0 & G_{31}^{*} \end{vmatrix} \tag{4}$$

Other material parameters in Eqs. (3) and (4) are the reduced shear moduluses for the softened concrete, G_{12}*, G_{23}* and G_{31}*, which can be defined by the equation:

$$G^{*}=\eta G \tag{5}$$

where G is the initial shear modulus of the uncracked concrete and η is the reduction coefficient. This coefficient is calculated here as:

$$\eta=1-\frac{\varepsilon_n^{*}}{\varepsilon_{\gamma\max}};\quad \eta\in[0,1]\quad for\ \varepsilon_n^{*}<\varepsilon_{\gamma\max},\qquad \eta=0\quad for\ \varepsilon_n^{*}\geq\varepsilon_{\gamma\max} \tag{6}$$

In case of the appearance of three cracks at one Gaussian point (in the directions 1, 2 and 3), it is necessary to correct the moduluses of elasticity according to Eq. (1) and the shear moduluses according to Eq. (5). When the values of strain exceed a prescribed maximal strain (ε_{max}) values in Gaussian points, one can assume that **D*** = 0 and that the failure of the material occurs.

2.2 Plasticity model for concrete

The non-linear behaviour of concrete for dominant compression stresses is described by an elasto-plastic material model based on the Mohr-Coulomb law. At multi-surface model presentation, the yielding surface is composed of six planes in the area of main stresses, defined by the following expressions:

$$\begin{aligned} f_1&=(\sigma_1-\sigma_3)+(\sigma_1+\sigma_3)\sin\varphi-2c\left(\bar{\varepsilon}^{p}\right)\cos\varphi \quad for\ \sigma_1>\sigma_2>\sigma_3\\ f_2&=(\sigma_2-\sigma_3)+(\sigma_2+\sigma_3)\sin\varphi-2c\left(\bar{\varepsilon}^{p}\right)\cos\varphi \quad for\ \sigma_2>\sigma_1>\sigma_3\\ f_3&=(\sigma_2-\sigma_1)+(\sigma_2+\sigma_1)\sin\varphi-2c\left(\bar{\varepsilon}^{p}\right)\cos\varphi \quad for\ \sigma_2>\sigma_3>\sigma_1\\ f_4&=(\sigma_3-\sigma_1)+(\sigma_3+\sigma_1)\sin\varphi-2c\left(\bar{\varepsilon}^{p}\right)\cos\varphi \quad for\ \sigma_3>\sigma_2>\sigma_1\\ f_5&=(\sigma_3-\sigma_2)+(\sigma_3+\sigma_2)\sin\varphi-2c\left(\bar{\varepsilon}^{p}\right)\cos\varphi \quad for\ \sigma_3>\sigma_1>\sigma_2\\ f_6&=(\sigma_1-\sigma_2)+(\sigma_1+\sigma_2)\sin\varphi-2c\left(\bar{\varepsilon}^{p}\right)\cos\varphi \quad for\ \sigma_1>\sigma_3>\sigma_2 \end{aligned} \tag{7}$$

Implementation of a multi-surface presentation of the model (Fig. 5) enables a rapid convergence of the mathematical procedure. For dominant compression stresses, a matrix of consistence is developed for each sextant separately. In Eq. (7), *c* is the function of equivalent accumulated plastic strains obtained from a uniaxial test and can be expressed as:

$$c(\bar{\varepsilon}^p) = \frac{1-\sin\varphi}{2\cos\varphi}\,\sigma\left(\bar{\varepsilon}^p\right) \tag{8}$$

where the relation between σ and $\bar{\varepsilon}^p$, proposed by Meschke [9], is given as:

$$\frac{\sigma(\bar{\varepsilon}^p)}{\sigma_c} = f_1(\bar{\varepsilon}^p) = c_y + (1-c_y)\sqrt{1-\left(\frac{\bar{\varepsilon}_c^p - \bar{\varepsilon}^p}{\bar{\varepsilon}_c^p}\right)^2} \tag{9}$$

where $\bar{\varepsilon}_c^p$ is the value of $\bar{\varepsilon}^p$ at $\sigma = \sigma_c$, and c_y is cohesion on the initial yield surface that bounds the initial elastic response. The coefficient c_y in Eq. (9) is equal to 0.52 according to [9]. Equation (9) defines the hardening rule.

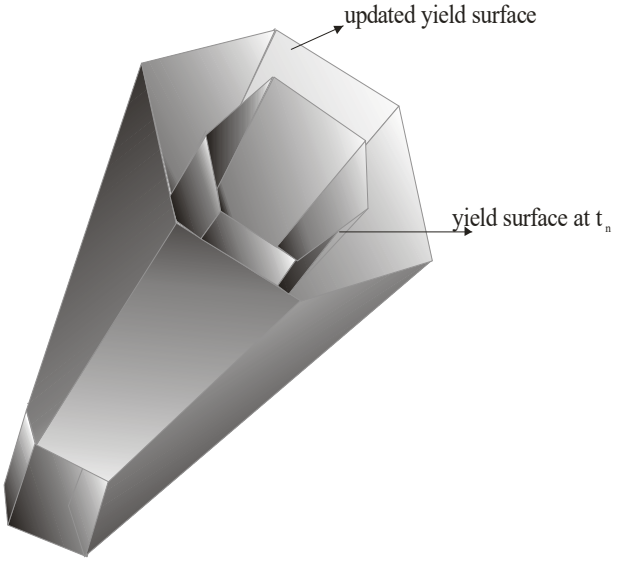

Figure 5. Triaxial presentation of the yield surface development defined by the hardening rule.

The softening law is controlled by the function for uniaxial compression, originally proposed by van Gysel and Taerwe [10] in the form:

$$\frac{\sigma(\bar{\varepsilon}^p)}{\sigma_c} = f_2(\bar{\varepsilon}^p) = \left[1+\left(\frac{n_1-1}{n_2-1}\right)^2\right]^{-2} \tag{10}$$

where $n_1 = \bar{\varepsilon}^p / \bar{\varepsilon}_c^p$ and $n_2 = (\bar{\varepsilon}_c^p + t)/\bar{\varepsilon}_c^p$. Parameter t controls the slope of the softening function. The complete elastic, hardening and softening functions of concrete with respect to the total plastic strains are presented in Fig. 6.

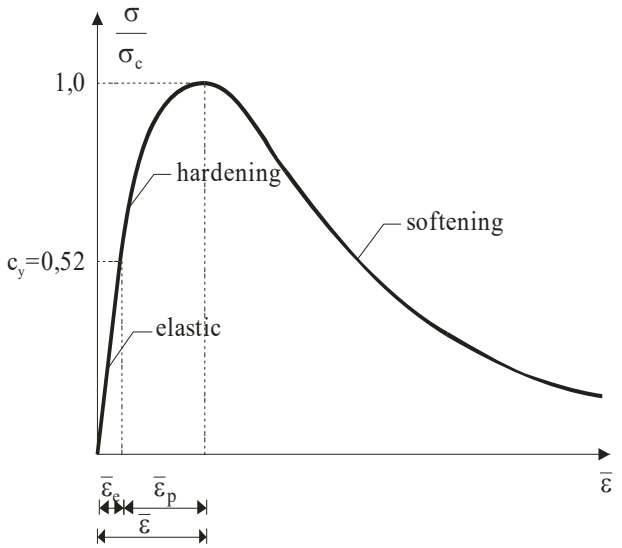

Figure 6. Hardening and softening functions with respect to the total plastic strains.

2.3 Material model of prestressed tendons

The non-linear behaviour of prestressed tendons is described by a 1D elasto-viscoplastic model. The tendon element geometry is described by a second order space function which is determined by its projections [4]. These elements make it possible to model arbitrarily curved prestressing tendons in space, therefore they can be determined independently of a 3D finite element mesh. This is very important in the case when the prestressing tendon cannot be located in one plane, (Fig. 7). The transfer of prestressing force onto the concrete is modelled numerically (Fig. 8).

Among losses influencing the decrease in the prestressing force, it is possible to compute the losses caused by friction and the ones resulting from the concrete deformations. The developed model makes it possible to compute prestressing structures in phases: before, during and after prestressing. The described models for concrete and reinforcement are implemented in a computer programme for a 3D analysis of the prestressed concrete structures where the structures are discretized by 3D finite elements with an embedded 1D element of prestressed tendons.

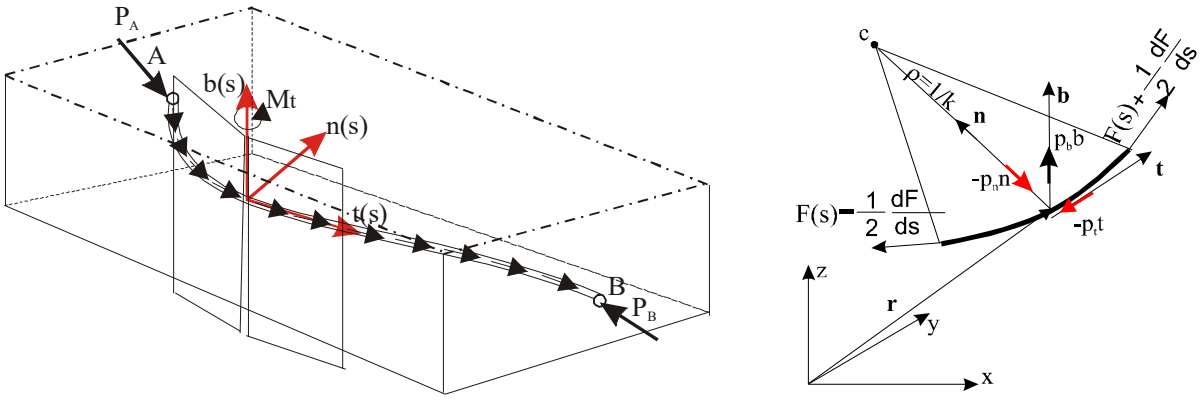

Figure 7. Space curvature of prestressing tendon.

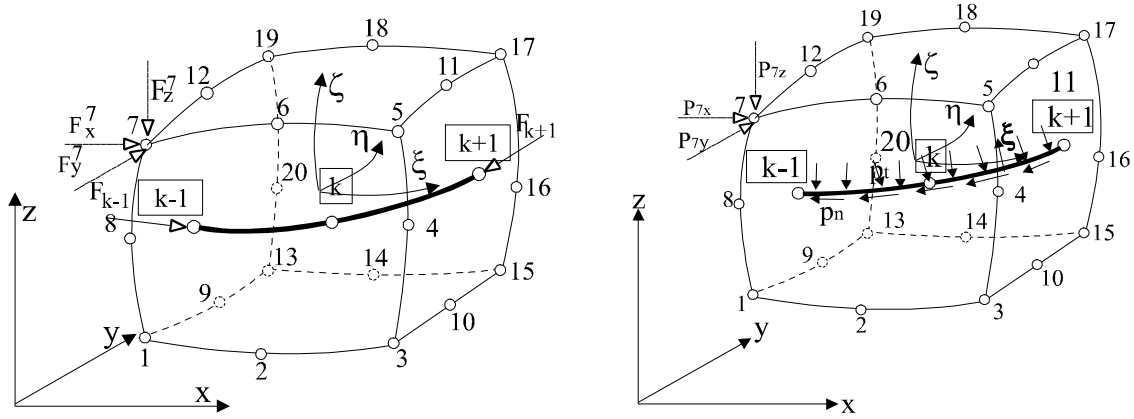

Figure 8. Numerical interpretation of prestressing force.

For a 3D analysis, the components that remain the same are:

$$P_x = \int_K \left(-p_n \frac{1}{\sqrt{\frac{d^2x}{ds^2}+\frac{d^2y}{ds^2}+\frac{d^2z}{ds^2}}} \rho \frac{d^2x}{ds^2} - p_t \frac{dx}{d\chi} \right) d\chi$$

$$P_y = \int_K \left(-p_n \frac{1}{\sqrt{\frac{d^2x}{ds^2}+\frac{d^2y}{ds^2}+\frac{d^2z}{ds^2}}} \rho \frac{d^2y}{ds^2} - p_t \frac{dy}{d\chi} \right) d\chi \quad (11)$$

$$P_z = \int_K \left(-p_n \frac{1}{\sqrt{\frac{d^2x}{ds^2}+\frac{d^2y}{ds^2}+\frac{d^2z}{ds^2}}} \rho \frac{d^2z}{ds^2} - p_t \frac{dz}{d\chi} \right) d\chi$$

Performing the Gaussian numerical integration of Eq. (11), one can obtain the values of the distributed load components along the tendon in the Gaussian points of the 1D tendon element ($P_x^{g.p.}$, $P_y^{g.p.}$ and $P_z^{g.p.}$).

To determine the influence of this distributed load along a 1D tendon element on the concrete element, it is necessary to map the coordinates of the Gaussian points from the global coordinate system to the local coordinate system of the parent concrete element. Finally, the components of the equivalent nodal forces due to the distributed load along the tendon defined in the global coordinate system can be expressed as:

$$P_x^i = \sum_{k=1}^{3} N_i(\xi_{g.p.}, \eta_{g.p.}, \zeta_{g.p.}) P_x^{g.p.}$$

$$P_y^i = \sum_{k=1}^{3} N_i(\xi_{g.p.}, \eta_{g.p.}, \zeta_{g.p.}) P_y^{g.p.} \quad (12)$$

$$P_z^i = \sum_{k=1}^{3} N_i(\xi_{g.p.}, \eta_{g.p.}, \zeta_{g.p.}) P_z^{g.p.}$$

3 Torsion of the tendons represented by space curvature

In the prestressed structures discretized with a 3D model, the tendon sometimes cannot be placed into one plane in all its length. The influences along the tendon appearing as effects of the tendon forces depend on the curvature of the tendon k(s), which is characterized by a deviation of the axis of the tendon from the tangent on the tendon and by the changes in the position of a binormal [4]. Binormals are not mutually parallel but form an angle ψ. The consequence of these changes is the torsion of the tendon φ, and it can be mathematically expressed as:

$$\varphi = \frac{d\psi}{ds} = \left| \frac{d\mathbf{b_0}}{ds} \right| \tag{13}$$

where ψ is the angle between unit vectors **b** and $\mathbf{b}_0$ of the binormals drawn in two considered neighbouring cross-sections.
The binormal can be expressed as:

$$\mathbf{b}_0 = \mathbf{t}_0 \times \mathbf{n}_0 \tag{14}$$

Deriving the vector product given by Eq. (14) across the length s of the arch, the following equation can be obtained:

$$\frac{d\mathbf{b}_0}{ds} = \mathbf{t}_0 \times \frac{d\mathbf{n}_0}{ds} - \mathbf{n}_0 \times \frac{d\mathbf{t}_0}{ds} \tag{15}$$

where $\frac{d\mathbf{t_0}}{ds}$ can be expressed as:

$$\frac{d\mathbf{t_0}}{ds} = \frac{d^2\mathbf{r}}{ds^2} = k(s)\mathbf{n_0} = \frac{\mathbf{n_0}}{\rho} \tag{16}$$

Introducing Eq. (16) into Eq. (15) one can obtain:

$$\frac{d\mathbf{b_0}}{ds} = \mathbf{t_0} \times \frac{d\mathbf{n_0}}{ds} \tag{17}$$

Considering the fact that the vector representing a derivation of the unit vector is perpendicular on it, one can conclude that the vector $\frac{d\mathbf{b}_0}{ds}$ is perpendicular on $\mathbf{b}_0$ i.e. on the binormal. The vector product is perpendicular on both vectors in vector product i.e. on $\mathbf{t}_0$ and $\frac{d\mathbf{n}_0}{ds}$, (see Eq. (17)). So, one can conclude that the vector $\frac{d\mathbf{b}_0}{ds}$ is perpendicular on tangent as well. As the vector is perpendicular both on binormal $\mathbf{b}_0$ and on tangent $\mathbf{t}_0$, it coincides with the principal normal vector $\mathbf{n}_0$ of the curve in the considered point and one can write:

$$\frac{d\mathbf{b_0}}{ds} = \left| \frac{d\mathbf{b_0}}{ds} \right| \mathbf{n}_0 \tag{18}$$

or according to Eq. (13):

$$\frac{d\mathbf{b}_0}{ds} = \pm\varphi\,\mathbf{n}_0 \tag{19}$$

The double sign in Eq. (19) appears because the vector $\frac{d\mathbf{b}_0}{ds}$ can have an identical or an opposite direction with respect to the vector $\mathbf{n}_0$. According to the sign convention, the torsion is positive if the rotation of the binormal is to the right regarding the unit vector of the tangent $\mathbf{t}_0$ while moving along the curve. Using the Frenet equation which shows the connection between the changes of the principal directions of the space curve, curvature k(s) and torsion, the torsion φ of the tendon in the considered cross-section can be expressed with scalar components of the vectors $\frac{dr}{ds}$, $\frac{d^2r}{ds^2}$ and $\frac{d^3r}{ds^3}$ as:

$$\varphi = \frac{-\begin{vmatrix} \frac{dx}{ds} & \frac{dy}{ds} & \frac{dz}{ds} \\ \frac{d^2x}{ds^2} & \frac{d^2y}{ds^2} & \frac{d^2z}{ds^2} \\ \frac{d^3x}{ds^3} & \frac{d^3y}{ds^3} & \frac{d^3z}{ds^3} \end{vmatrix}}{\left(\frac{d^2x}{ds^2}\right)^2 + \left(\frac{d^2y}{ds^2}\right)^2 + \left(\frac{d^2z}{ds^2}\right)^2} \tag{20}$$

4 Numerical examples

The described modelling of the concrete and prestressing tendons is implemented in the

computer programme PRECON3D [1] and [2]. The prestressed beams and/or girders used in everyday engineering structures generally have I, T, Π or similar cross-sections. Beams and/or girders with such cross-sections, due to an apparent three-dimensional stress state, cannot be accurately analyzed with a two-dimensional model.

The proposed three-dimensional numerical model, PRECON3D, is validated and compared with known experimental and/or analytical results on two examples: (i) four point bending of normal-strength and high-strength reinforced concrete beams with four different constant-zone lengths and two different reinforcement ratios taken from Ref. [11] on which, also, the mesh size effect have been analyzed; (ii) three point bending of reinforced concrete beam taken from [12]; (iii) prestressed concrete beam taken from [13]; (iv) prestressed Π-beam taken from [14].

4.1 Four point bending of rc beams

The example of four point bending of reinforced concrete beams have been performed according to the experimental testing by Weiss et al. [11] and mechanical two-dimensional model by Fantilli et al. [15] where 16 simply supported reinforced concrete beams were tested under four point bending. These 16 beams were grouped in four groups of beams, having different concrete strength (high strength concrete HSC or normal strength concrete NSC), different percentage of reinforcement (high ratio HR or low ratio LR) and four different lengths (1*d*, 2*d*, 3*d* and 4*d*). Each group contains four beams with the same cross-section but different constant-moment zone length *L* (respectively 1, 2, 3 and 4 times the effective depth *d* of the cross-section). The geometry of tested beams is shown in Fig. 9.

The main material characteristics and the amount of steel reinforcement are summarised in Table 1 according to Weiss et al. [11].

The tested beams are discretized with three-dimensional 20-node finite elements describing concrete body with embedded one-dimensional 3-node finite elements describing the reinforcement. Two finite element meshes were used: (i) mesh A: coarse mesh shown in Fig. 10; and (ii) mesh B: fine mesh obtained by dividing elements from mesh A on half over the height, i.e. mesh B has double number of elements describing concrete body.

According to the performed numerical tests [16] with the developed computer programme PRECON3D [1], a correlation between ductility and constant-moment zone length *L* is shown for the beam of normal strength concrete (NSC) with low (LR) and high (HR) reinforcement ratio in Fig. 11 and for the beam of high strength concrete (HSC) with low (LR) and high (HR) reinforcement ratio in Fig. 12.

In Figures 11 and 12, the value of moment *M* in constant-moment zone length *L* is obtained as $F \cdot 5d$ while ε represents the mean compressive top fibre strains in constant-moment zone length *L*. Fantilli et al. [15] stated that a strict correlation between the ductility and constant-moment zone length *L* is obtained by numerical results of his model. They also stated that only a little discrepancy is revealed for beams HSC-LR, made of high strength concrete and low reinforcement ratio (Fig. 12), for which the maximum bending moment and ductility are overestimated.

The obtained numerical results (green and purple lines in Fig. 11 and 12) [1] and [16] show better correlation with experimental results (red lines) [11] for both meshes, coarse and fine one, than the one presented by Fantilli et al. (blue lines) [15]. The difference in numerical results obtained for these two meshes (mesh A: coarse; mesh B: fine) is practically negligible.

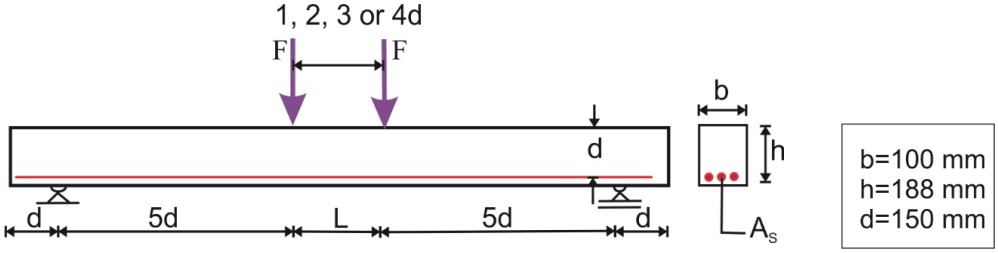

Figure 9. The beam tested by Weiss et al. [11]: static conditions and geometrical characteristics.

Table 1. Material characteristics of the beam tested by Weiss et al. [11] (see Fig. 9)

Beams	f_c (MPa)	E_c (MPa)	A_s (mm^2)	f_y (MPa)	f_u (MPa)	E_s (MPa)	L/d
NSC-LR-1D	39.8	32 500	138.8	395	557	192 000	1
NSC-LR-2D	46.6	32 000	138.8	395	557	192 000	2
NSC-LR-3D	46.6	32 000	138.8	395	557	192 000	3
NSC-LR-4D	39.8	32 500	138.8	395	557	192 000	4
NSC-HR-1D	38.7	32 700	382.3	400	634	204 000	1
NSC-HR-2D	38.7	31 500	382.3	400	634	204 000	2
NSC-HR-3D	46.7	32 300	382.3	400	634	204 000	3
NSC-HR-4D	46.7	32 300	382.3	400	634	204 000	4
HSC-LR-1D	98.8	34 300	382.3	400	634	204 000	1
HSC-LR-2D	100.6	36 300	382.3	400	634	204 000	2
HSC-LR-3D	100.6	36 300	382.3	400	634	204 000	3
HSC-LR-4D	98.8	34 300	382.3	400	634	204 000	4
HSC-HR-1D	108.3	36 800	981.8	431	614	203 000	1
HSC-HR-2D	97.9	35 400	981.8	431	614	203 000	2
HSC-HR-3D	97.9	35 400	981.8	431	614	203 000	3
HSC-HR-4D	108.3	36 800	981.8	431	614	203 000	4

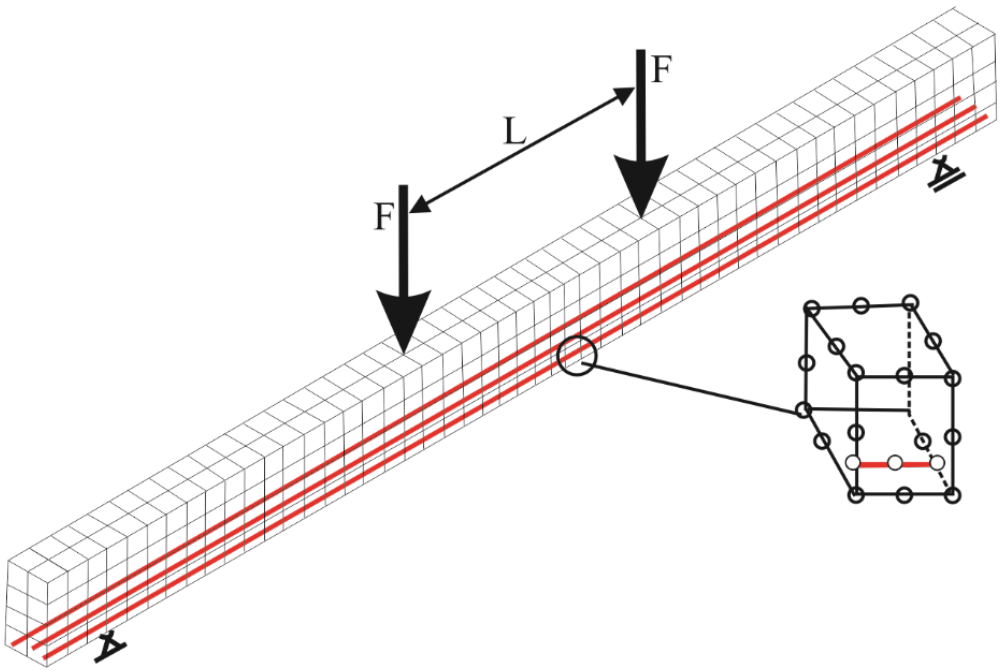

Figure 10. Numerical discretization of the beam, tested by Weiss et al. [11], for the programme PRECON3D [1]: coarse mesh.

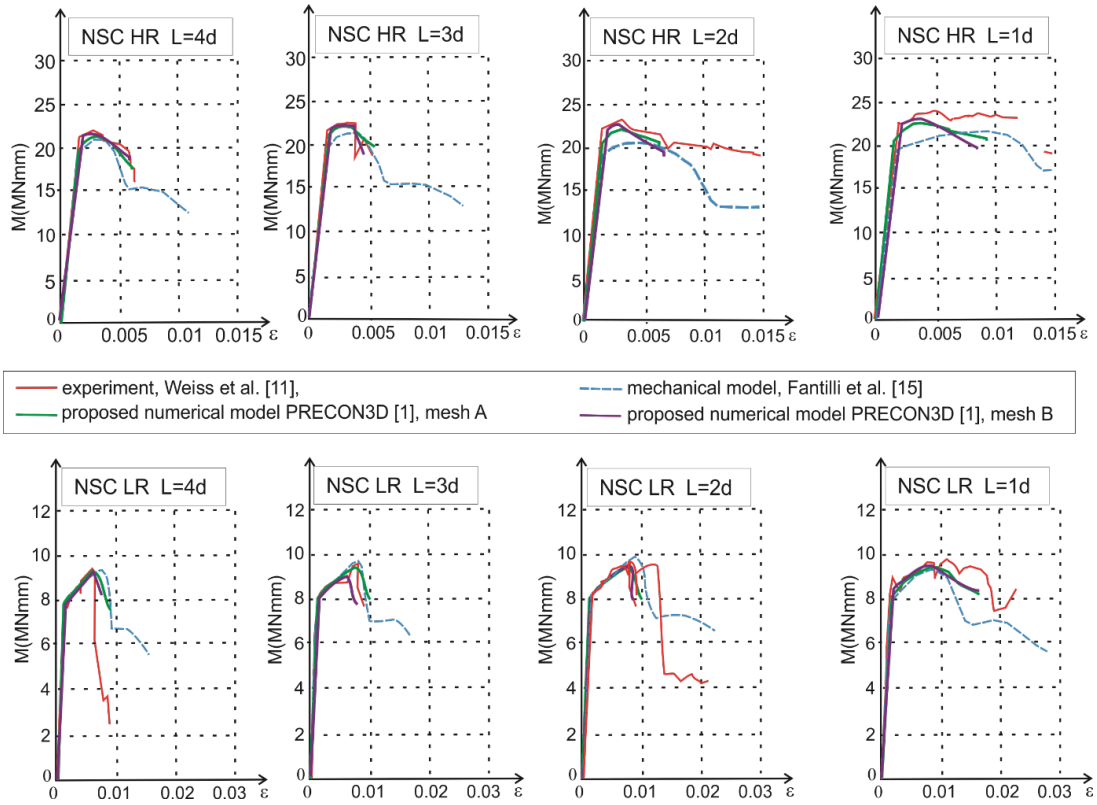

Figure 11. Comparison between the numerical results of the proposed model PRECON3D [1], mechanical model [15] and those experimentally measured in Ref. [11] for NSC beams.

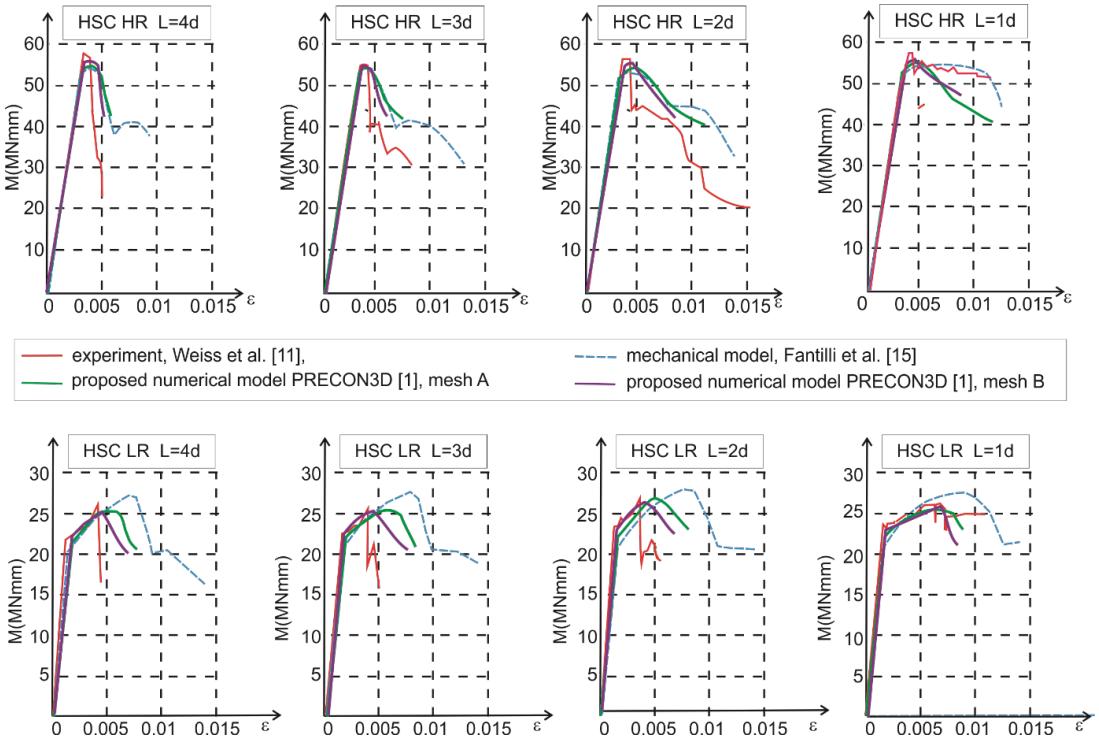

Figure 12. Comparison between the numerical results of the proposed model PRECON3D [1], mechanical model [15] and those experimentally measured in Ref. [11] for HSC beams.

4.2 Three point bending of rc beam

The example of three point bending of reinforced concrete beams have been performed according to the numerical testing by Rabczuk and Belytschko [12] and experimental testing by Bosco and Debernardi [17] where two simply supported reinforced concrete beams were tested under three point bending. The test setup and the dimensions of two tested beams marked T5A1 and T6A1 are shown in Fig. 13. As can be seen from Fig. 13, the beam T6A1 has a higher degree of reinforcement at the bottom than beam T5A1.

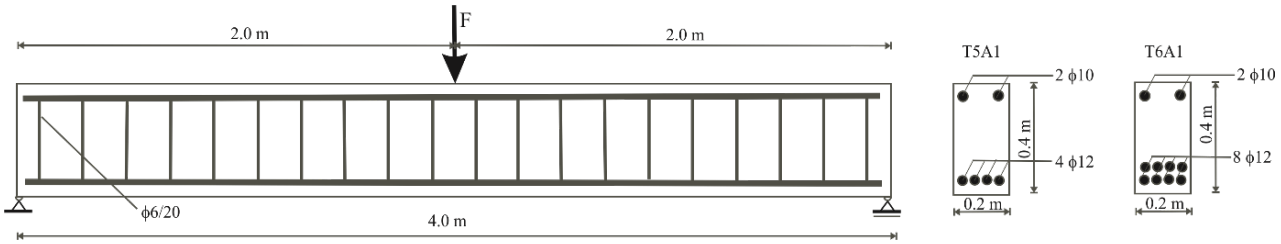

Figure 13. The test setup and the dimensions of the beams T5A1 and T6A1 [12].

The material characteristics of the reinforced concrete beams are [12]: (i) concrete: the modulus of elasticity, E_c = 28 000 N/mm^2; Poisson's ratio, ν = 0.22; the uniaxial compressive strength, σ'_c = 32.0 N/mm^2; the uniaxial tensile strength, σ_t = 2.5 N/mm^2; fracture energy, G_f = 100 N/m; (ii) reinforcement: the uniaxial tensile strength, σ_M = 672 N/mm^2; uniaxial yield strength, σ_y = 587 N/mm^2; the modulus of elasticity, E_s = 200 000 N/mm^2.

The tested beams are discretized with three-dimensional 20-node finite elements describing concrete body with embedded one-dimensional 3-node finite elements describing the longitudinal reinforcement and stirrups.

Due to the obtained results from previous example considering mesh dependence where that influence was almost negligible, only one mesh was used in this example.

The load - mid displacement curves are shown in Fig. 14. The agreement between the experiments [17], computational results [12] and the one obtained by computer programme PRECON3D [1] is excellent. The difference of the reinforcement at the bottom of the beams T6A1 and T5A1 (8ϕ12 versus 4ϕ12) causes different failure patterns. The beam T5A1 failed due to plastic flow of the lower reinforcement. The beam T6A1 failed due to the failure of the concrete compression zone in the middle upper part of the beam. For beam T6A1, a high damage compression zone caused a rapid decrease in the slope of the load – mid displacement curve (Fig. 14).

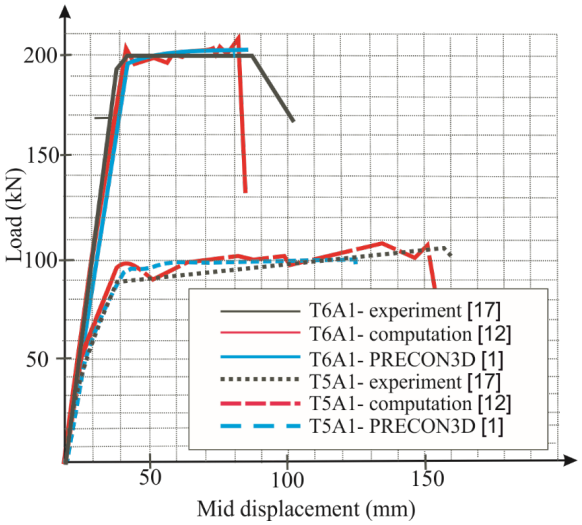

Figure 14. The load – mid displacement curves of the beams T5A1 and T6A1.

4.3 Prestressed concrete beam

As an example of a three point bending of a prestressed concrete beam, a beam marked 16/31-1865 numerically analyzed by Ayoub and Filippou [13] was chosen to perform bond-slip analysis (Fig. 15).

Ayoub and Filippou [13] analyzed two bond-slip situations: (i) full bond; and (ii) bond-slip described by special bond element that describes the transfer of stresses between the prestressing tendons and the concrete. A developed model incorporated into computer programme PRECON3D [1, 2] considers only a full bond.

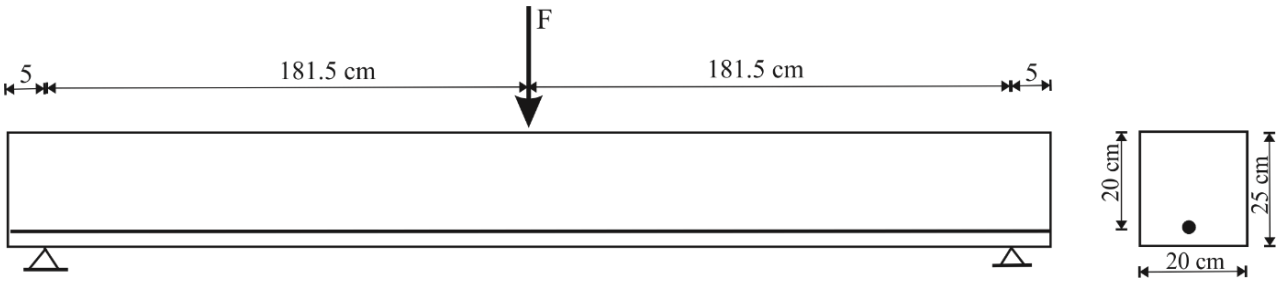

Figure 15. The test setup and the dimensions of the beam 16/31-1865 [13].

The material characteristics of the prestressed concrete beam 16/31-1865 according to [13] are: (i) concrete: the modulus of elasticity, E_c = 35 000 N/mm^2; Poisson's ratio, ν = 0.20; the uniaxial compressive strength, σ'_c = 31.0 N/mm^2; the uniaxial tensile strength, σ_t = 3.1 N/mm^2; (ii) tendon: the modulus of elasticity, E_s = 204 900 N/mm^2; uniaxial yield strength, σ_y = 1 639.3 N/mm^2; the cross-section area of the prestressed tendon, A_p = 146.4 mm^2; the initial prestressing force, F_p = 188.27 kN.

The global response, i.e. the load – mid displacement curves of the beam 16/31-1865 are shown in Fig. 16. The agreement between the results obtained by computer programme PRECON3D [1] and the one obtained by Ayoub and Filippou [13] is excellent, especially considering negligible difference between results calculated for full-bond and bond-slip cases.

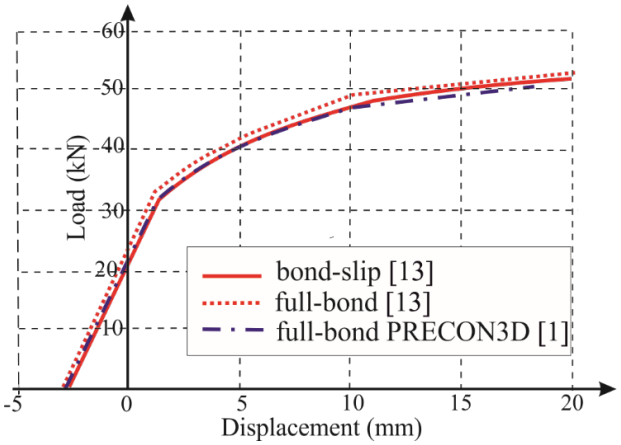

Figure 16. Global response of beam 16/31-1865.

As can be seen from Fig. 16, general behavior of prestressed beam 16/31-1865 is almost identical for all three analyses. Before the application of the load, the displacement caused only by prestressed force shows a negative value, referred to as camber. Yielding of the tendon starts at a load value of 32 kN. The beam then shows a ductile behavior up to the collapse. For the validation of the developed model, obtained results are compared with ones available from [13]: the calculated maximum tendon strain was 0.0178 versus 0.0187, which corresponds to a stress in the tendon of 1 705 MPa versus 1 716 MPa; flexural crushing occurs at a maximum moment of 45.3 kNm versus 46.6 kNm, which corresponds to loading force (F) 49.95 kN versus 51.35 kN.

4.4 Prestressed Π-beam

The analyzed prestressed Π-beam is taken from [14]. The beam has been tested experimentally [14] and the results have been compared with the numerical ones obtained by computer programme PRECON3D [1]. The prestressed Π-beam geometry and loading are shown in Fig. 17.

The material characteristics of the prestressed Π-beam are [14]: the modulus of elasticity of the concrete, E_c = 36 000 N/mm^2; Poisson's ratio of the concrete, ν = 0.25; the uniaxial compressive strength of the concrete, σ'_c = 53.1 N/mm^2; the uniaxial tensile strength of the concrete, σ_t = 7.4 N/mm^2; the compressive strain of the concrete, ε_c = 0.0035; the tensile strain of the concrete, ε_t = 0.002; tensile correction coefficient, α = 0.6; the uniaxial tensile strength of the steel, σ_y = 1 900 N/mm^2; the modulus of elasticity of the steel, E_s = 195 000 N/mm^2; yielding strain of the steel, ε_y = 0.010; and the total cross-section area of the prestressed tendons, A_s = 614 mm^2.

The prestressed Π-beam concrete structure is discretized with two meshes: (i) coarse mesh: 104 three-dimensional, 20-node finite elements describing concrete body and with 13 one-dimensional, 3-node finite elements for each tendon (Fig. 18); (ii) fine mesh: 208 three-dimensional, 20-node finite elements describing concrete body and

with 13 one-dimensional, 3-node finite elements for each tendon.

The load-deflection diagrams of the mid-span point, under a concentrated force at the mid-span, up to the failure for both meshes are presented in Fig. 19.

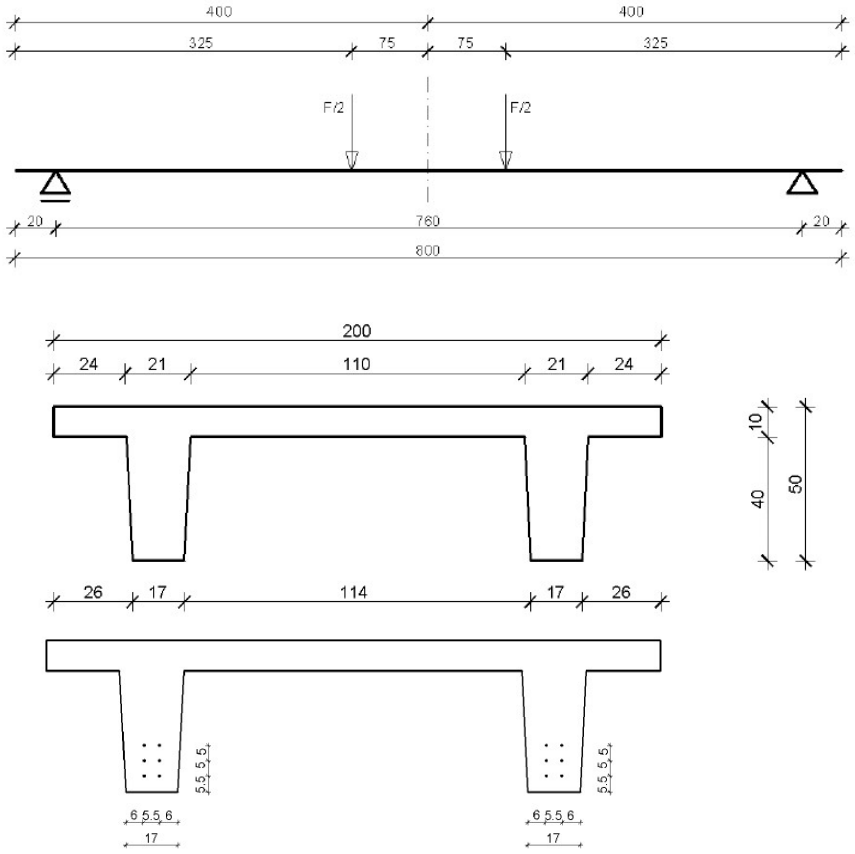

Figure 17. The Π –beam static conditions, geometry and loading [14].

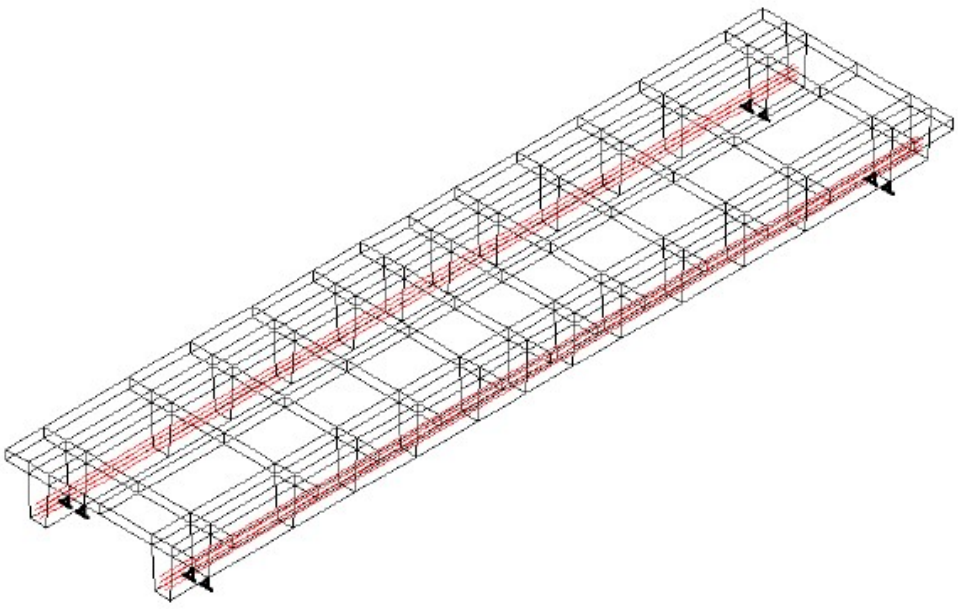

Figure 18. The prestressed Π-beam finite element discretization.

As can be seen from Fig. 19, the influence of mesh size is evident. Finer mesh gives better results: (i) before the application of the load, the displacement caused by prestressing shows a negative value almost identical as a camber in the experiment [14]; (ii) load – displacement curve obtained by finer mesh is closer to the experimental one than the one obtained by coarser mesh; (iii) yielding is better described by finer mesh (closer to the experimental results).

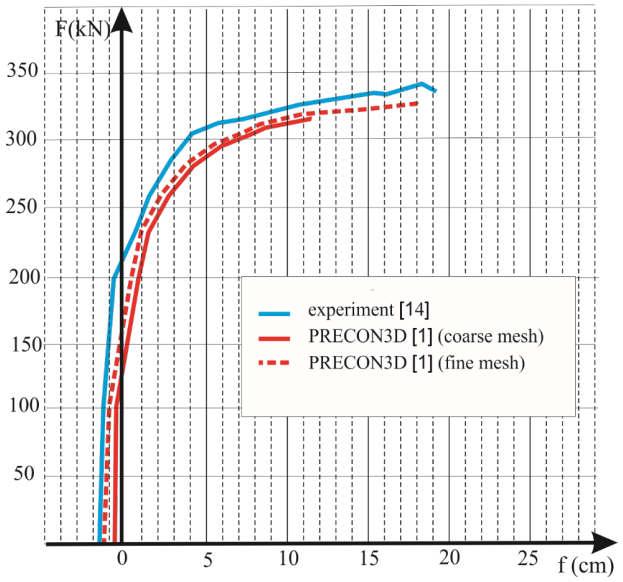

Figure 19. The load-deflection diagram of the mid-span point.

Furthermore, developed computer programme PRECON3D [1, 2], among other modelling possibilities, enables the calculation of stresses in concrete and steel in characteristic points, deformed shapes of a structure in all phases, and the losses of a prestressed force caused by elastic shrinkage of concrete. Some other analyzed examples of reinforced concrete and prestressed concrete structures, possibilities and comparisons can be found in [2], [3] and [16].

5 Conclusions

This paper presents a three-dimensional non-linear material model for concrete based on the modified Mohr-Coulomb law for dominant compression stresses and the modified Rankine law for dominant tensile stresses. Non-linear triaxial behaviour of concrete includes all dominant influences. The model is defined by elementary material parameters, describing thus a very complex behaviour of reinforced and prestressed concrete structures as simply and effectively as possible.

The obtained results show good agreement with the ones found in literature, both experimentally and numerically. Considering performed mesh sensitivity analyses, it can be stated that finer mesh versus coarse one gives generally better results, especially in the analysis of yielding zones of prestressed concrete structures.

Analyses carried out by numerical programme PRECON3D can be used as a numerical test for loading the structures until collapse. The results obtained in this study show very good agreement with the experimental data and accuracy falls within an interval of 5-8% (the model is always on the side of safety). So, these numerical tests can be used for the computation of the bearing capacity of new and existing structures. In this way, the expensive experimental tests can be reduced.

Acknowledgement

The financial support provided by the Ministry of Science, Education and Sports of the Republic of Croatia under the projects *Numerical and Experimental Modelling of Engineering Structures*, Grant No. 0083061, and *Numerical and Experimental Investigations of Engineering Structures Behaviour*, Grant No. 083-0831541-1547, as well as financial support provided by the Faculty of Civil Engineering, Architecture and Geodesy of the University of Split under the individual overhead support scheme is gratefully acknowledged.

References

[1] Galić, M., Marović, P., Nikolić, Ž.: PRECON-3D – Computer programme for 3D analysis of engineering structures, University of Split, Faculty of Civil Engineering, Architecture and Geodesy, Split, 2005.

[2] Galić, M.: *Development of nonlinear numerical 3D model of reinforced and pre-stressed concrete structures*, Ph.D. Thesis, University of Split, Faculty of Civil Engineering, Architecture and Geodesy, Split, 2006.

[3] Galić, M., Marović, P., Nikolić, Ž.: *Modified Mohr-Coulomb – Rankine Material Model for*

Concrete, Engineering Computations, 28 (2011), 7, 853-887.

[4] Galić, M., Marović, P., Nikolić, Ž.: *Mathematical Formulation of the Space Curvature of the Tendon in the PC Structures*, International Journal for Engineering Modelling, 21 (2008), 1-4, 15-22.

[5] Marović, P., Nikolić, Ž., Galić, M.: *Some Aspects of 2D and/or 3D Numerical Modelling of Reinforced and Prestressed Concrete Structures*, Engineering Computations, 22 (2005), 5/6, 684-710.

[6] Cervera, M.: *Nonlinear analysis of reinforced concrete structures using three dimensional and shell finite element models*, Ph.D. Thesis, University of Wales, Swansea, 2006.

[7] *CEB-FIP Model Code for Concrete Structures*, Bulletin d'information 144, Euro-International Committee for Concrete, 1978.

[8] Damjanić, F.B.: *Reinforced concrete failure prediction under both static and transient conditions*, Ph.D. Thesis, University College of Swansea, Swansea, 1983.

[9] Meschke, G.: *Synthese aus konstitutiven Modelieren von Beton mittels dreiaxialer, elasto-plasticher Werkstoffmodelle und Finite-Elemente-Analysen dickwandiger Stahlbeton-konstruktionen*, Ph.D. Thesis, Vienna University of Technology, Vienna, 1989.

[10] van Gysel, A., Taerwe, L.: *Analytical Formulation of the Complete Stress-Strain Curve for High Strength Concrete*, Materials and Structures, 29 (1996), 193, 529-533.

[11] Weiss, W.J., Guler, K., Shah, S.P.: *Localization and Size-dependent Response of Reinforced Concrete Beams*, ACI Structural Journal, 98 (2001), 5, 686-695.

[12] Rabczuk, T., Belytschko, T.: *Application of Particle Methods to Static Fracture of Reinforced Concrete Structures*, International Journal of Fracture, 137 (2006), 1-4, 19-49.

[13] Ayoub, A., Filippou, F.C.: *Finite-Element Model for Pretensioned Prestressed Concrete Girders*, ASCE Journal of Structural Engineering, 136 (2010), 4, 401-409.

[14] Markić, R.: *Influence of relation of prestressed and classical reinforcement on the behavior of concrete beam structures*, Ph.D. Thesis, University of Split, Faculty of Civil Engineering, Architecture and Geodesy, Split, 2012.

[15] Fantilli, A.P., Iori, I., Vallini, P.: *Size Effect of Compressed Concrete in Four Point Bending RC Beams*, Engineering Fracture Mechanics, 74 (2007), 1, 97-108.

[16] Galić, M., Marović, P., Harapin, A.: *Parametric Analysis of Constant-Moment Zone Length in Four Point Bending of Reinforced Concrete Beams*, Materialwissenschaft und Werkstoff-technik, 44 (2013), 5, 449-457.

[17] Bosco, C., Debernardi, P.G.: Experimental investigations on the ultimate rotational capacity of R.C. beams, Politecnico di Torino, Dipartimento di Ingegneria Structurale, 1992.